RESEARCH ARTICLE

# Monosomic Loss of MIR15A/MIR16-1 Is a Driver of Multiple Myeloma Proliferation and Disease Progression

Marta Chesi[1], Caleb K. Stein[1], Victoria M. Garbitt[1], Meaghen E. Sharik[1], Yan W. Asmann[2], Matteo Bergsagel[1], Daniel L. Riggs[1], Seth J. Welsh[1], Erin W. Meermeier[1], Shaji K. Kumar[3], Esteban Braggio[1], and P. Leif Bergsagel[1]

## ABSTRACT

The most common genetic abnormality in multiple myeloma is the deletion of chromosome 13, seen in almost half of newly diagnosed patients. Unlike chronic lymphocytic leukemia, where a recurrent minimally deleted region including *MIR15A/MIR16-1* has been mapped, the deletions in multiple myeloma predominantly involve the entire chromosome and no specific driver gene has been identified. Additional candidate loci include *RB1* and *DIS3*, but while biallelic deletion of *RB1* is associated with disease progression, *DIS3* is a common essential gene and complete inactivation is not observed. The Vk*MYC transgenic mouse model of multiple myeloma spontaneously acquires del(14), syntenic to human chromosome 13, and *Rb1* complete inactivation, but not *Dis3* mutations. Taking advantage of this model, we explored the role in multiple myeloma initiation and progression of two candidate loci on chromosome 13: *RB1* and *MIR15A/MIR16-1*. Monoallelic deletion of *Mir15a/Mir16-1*, but not *Rb1*, was sufficient to accelerate the development of monoclonal gammopathy in wild-type mice and the progression of multiple myeloma in Vk*MYC mice, resulting in increased expression of *Mir15a/Mir16-1* target genes and plasma cell proliferation, which was similarly observed in patients with multiple myeloma.

**SIGNIFICANCE:** In the absence of a defined, minimally deleted region the significance of del(13) in multiple myeloma has remained controversial. Here we show that haploinsufficiency *of Mir15a/Mir16-1*, but not *Rb1*, upregulates the cell cycle–regulatory network, inducing monoclonal gammopathy in mice and promoting multiple myeloma progression in both mice and men.

*See related commentary by Walker, p. 16.*

## INTRODUCTION

Multiple myeloma is a tumor of monoclonal antibody (mAb) producing plasma cells (PC) in the bone marrow (BM). It is preceded by a common premalignant condition called monoclonal gammopathy of undetermined significance (MGUS) that shares with multiple myeloma the presence of recurrent chromosomal translocations to the immunoglobulin loci, resulting in dysregulated expression of D-type Cyclins (*CCND1–3*), *NSD2/MMSET* and *FGFR3*, the MAF family of

[1]Division of Hematology and Medical Oncology, Mayo Clinic, Scottsdale, Arizona. [2]Division of Health Science Research, Mayo Clinic, Jacksonville, Florida. [3]Division of Hematology and Medical Oncology, Mayo Clinic, Rochester, Minnesota.

**Note:** Supplementary data for this article are available at Blood Cancer Discovery Online https://bloodcancerdiscov.aacrjournals.org/.

**Corresponding Author:** Marta Chesi, Mayo Clinic, 13400 East Shea Boulevard, Scottsdale, AZ 85259. Phone: 480-301-4703; Fax: 480-301-8387; E-mail: chesi.marta@mayo.edu

Blood Cancer Discov 2020;1:68–81

**doi:** 10.1158/2643-3249.BCD-19-0068

transcription factors (*MAF, MAFA* and *MAFB*), or hyperdiploidy of odd numbered chromosomes, both considered primary, tumor-initiating events (1).

We have shown that overexpression of *MYC* and *MYC* target genes distinguishes MGUS from patients with multiple myeloma (2–4). Rearrangements of the *MYC* locus occur in approximately 40% of patients with multiple myeloma and result in *MYC*-dysregulated expression, driven by a variety of juxtaposed enhancers and super-enhancers active in PCs (5). By forcing sporadic *MYC* activation in germinal center B cells of C57BL/6 mice, we generated a clinically predictive and biologically faithful transgenic mouse model of multiple myeloma, Vk*MYC, characterized by a progressive monoclonal PC expansion in the BM associated with the presence of abundant monoclonal immunoglobulins detectable on serum protein electrophoresis as an M-spike, as well as anemia, bone disease, and renal impairment (2, 6–8). Notably, no multiple myeloma develops in Vk*MYC mice when backcrossed from a C57BL/6 strain, prone to develop MGUS, to a Balb/c strain that does not, indicating that *MYC* dysregulation is not an MGUS-initiating event but rather drives the progression of MGUS to multiple myeloma (5). Additional genetic events are involved in multiple myeloma progression and the most common include activating mutations of genes in the RAS and MAPK or NFκB pathways, or inactivation of tumor suppressor genes like *DIS3, FAM46C, RB1, CDKN2C*, or *TP53* (9).

Monosomy 13, or del(13q), occurs in approximately 40% of patients with multiple myeloma, but is found at much higher frequency in patients with t(4;14) translocations (80%–94%) or MAF family translocations (75%–80%), both considered high-risk features (10, 11). The prognostic significance of monosomy 13 remains controversial, with earlier studies indicating a lack of evidence for independent association with increased risk (12) and a more recent study showing shorter overall survival (OS) in patients with monosomy 13, even after adjusting for age, sex, International Staging System (ISS) stage, first-line therapy, and high-risk features (11).

In chronic lymphocytic leukemia (CLL) and its precursor condition, monoclonal B-cell lymphocytosis, the chromosome 13 deletion is found in 58% and 39% of cases, respectively, with a minimally deleted region (MDR) mapped to 13q14 (13). In contrast, no MDR has been identified in multiple myeloma, and most of the tumors with chromosome 13 deletion do not have mutations of *RB1* or *DIS3* (the two genes on chromosome 13 recurrently mutated in multiple myeloma). This suggests that haploinsufficiency of one or more tumor suppressor genes drives the loss of chromosome 13 in this disease (14).

The *MIR15A/MIR16-1* cluster is located within the CLL 13q14 MDR and it has been shown to directly regulate the expression of several cell cycle–controlling genes (*CCND1–3, CDK4* and *6, CHK1, MCM5*, and *CDC25A*). Consistently, loss of *MIR15A/MIR16-1* drives B-cell expansion *in vitro* and *in vivo* by promoting $G_0$–$G_1$–S transition in both murine and human B cells and PCs (15–17). Furthermore, *Mir-15a/16-1*$^{null}$ mice develop lymphoproliferative pathologies, although with low penetrance and indolent disease course. A minority of mice also develop tumors with plasmacytic features, suggesting a role for *MIR15A/MIR16-1* deletion in PC tumorigenesis (15). Here, we take advantage of available mouse strains and examine *in vivo* the impact of two candidate loci on chromosome 13, *RB1* and *MIR15A/MIR16-1*, and their respective contributions to gene expression and tumor progression in Vk*MYC mice and in a large cohorts of MGUS and multiple myeloma patients observed at Mayo Clinic or enrolled in the CoMMpass clinical trial (http://research.themmrf.org).

## RESULTS

### Frequent Monosomy 14 and Focal *Rb1* Deletion in Vk*MYC Mice

To investigate the genomic alterations that cooperate with *MYC* in driving multiple myeloma progression, we performed array-based comparative genomic hybridization (aCGH) analysis on 26 independent CD138-selected multiple myeloma tumors from 17 aged Vk*MYC mice (*de novo* tumors) and 9 Vk*MYC tumor–bearing mice (transplants) using the mouse Agilent 244K array (Fig. 1A). Visual identification of biallelic deletions within the IgH locus, physiologically occurring during B-cell development (18), confirmed the flow cytometric estimation of purity (>85%) for all but one sample (Supplementary Fig. S1A). Overall, the genetic complexity of Vk*MYC tumors is low. Like human multiple myeloma, a common abnormality identified in Vk*MYC multiple myeloma was loss of a sex chromosome: 7 of 12 male and 9 of 14 female mice had loss of Y and X, respectively. Although we found no evidence of hyperdiploidy, present in approximately 50% of human patients with multiple myeloma, we detected frequent copy number gains of chromosomes 1, 6, 16, and 18 in three, three, two, and two tumors, respectively. We also noted monosomy of chromosomes 5 and 14 in 13 and six tumors, respectively. In particular, the mouse chromosome 14 has a large MDR syntenic to the human chromosome 13, which includes *Dis3, Rb1*, and the *Mir15a/Mir16-1* cluster. Of the six cases with monosomy 14, two had focal *Rb1* biallelic deletions. In addition, one tumor without monosomy 14 presented with focal biallelic *Rb1* and monoallelic *Mir15a/Mir16-1* deletion and another tumor with monoallelic *Mir15a/Mir16-1* loss (Fig. 1B). Additional recurrent focal biallelic deletions identified in Vk*MYC tumors include *Kdm6a/Utx,* found in seven tumors (Supplementary Fig. S1B), and *Cdkn2a*, found in two tumors (Supplementary Fig. S1C). The summary of recurrent chromosome copy-number abnormalities (CNA) and biallelic deletions detected in Vk*MYC tumors is reported in Table 1. While a complete analysis of genomic aberrations in Vk*MYC multiple myeloma is ongoing, a focused examination of candidate genes on mouse chromosome 14 did not identify any single-nucleotide variants (SNV) of *Rb1, Dis3*, or *Mir15a/Mir16-1* in 29 independent tumors.

### Analysis of Human Multiple Myeloma Identifies a Similar Frequency of *DIS3* Mutation at Diagnosis and Relapse, but Increased Frequency of *RB1* Inactivation with Disease Progression

Analysis of patients with multiple myeloma enrolled in the CoMMpass study identified nonsynonymous (NS) SNV of *DIS3*

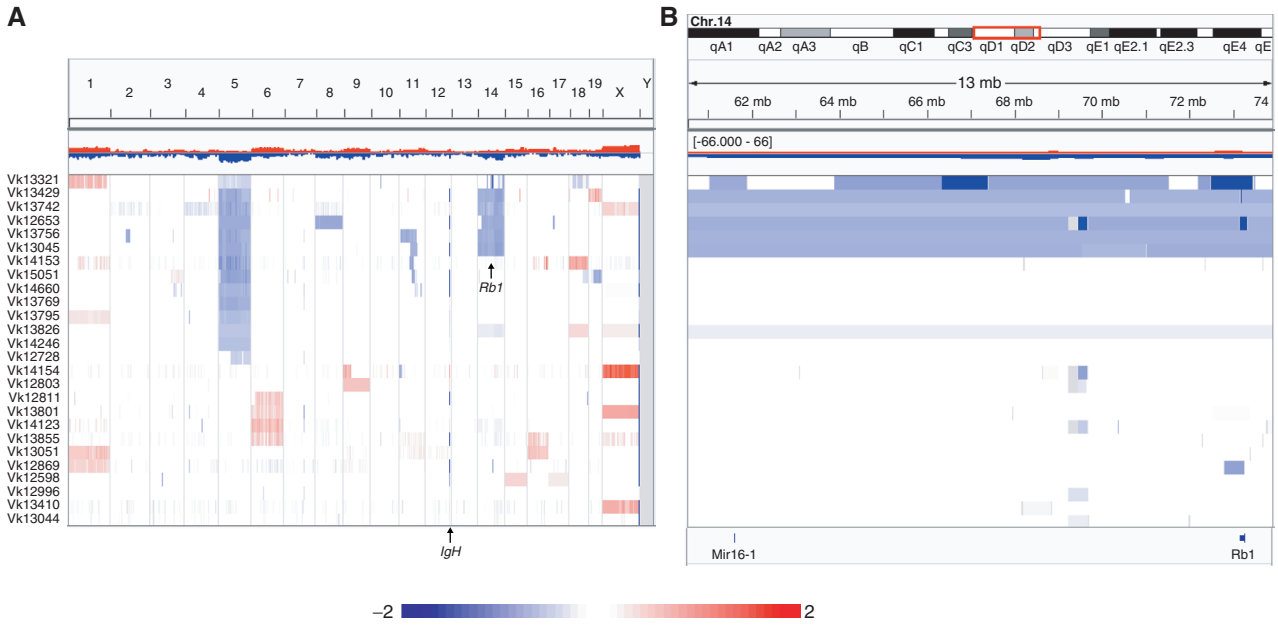


**Figure 1.** Recurrent monosomy 14, syntenic to human chromosome 13, and *Rb1* focal deletions in multiple myeloma tumors from Vk*MYC mice. Graphic representation in IGV of copy number abnormalities detected by aCGH in 26 independent CD138+ multiple myeloma tumors from Vk*MYC mice shown at whole genome level (**A**) or zoomed on the *Mir15a/16-1* and *Rb1* loci on chromosome 14 (**B**). Red and blue indicate copy number gain and loss, respectively, and color scale ($log_2$) is indicated. Each line represents an individual tumor sample.

in 10% of both newly diagnosed multiple myeloma (NDMM) and relapsed multiple myeloma (RMM) cases. These were almost exclusively missense mutations, with no nonsense or frameshift mutations, no copy-neutral loss of heterozygosity, or biallelic deletions. A third of the mutations occurred in three codons (D479, D488, and R780), almost never associated with del(13) (Fig. 2A). In contrast, the remaining two-thirds of *DIS3* mutations were distributed across the various exons, almost always associated with del(13). Furthermore, the Dependency Map (http://depmap.org) identifies *DIS3* as a common essential gene across almost all cell lines examined, indicating that complete inactivation is not tolerated. Altogether, this analysis highlights a complicated relationship between different *DIS3* mutations and del(13). In contrast, NS-SNV of *RB1* were predominantly truncating (10/19 NS-SNV are stop-gain or frameshift) and biallelic inactivation of *RB1* [NS-SNV with loss of heterozygosity (LOH) or biallelic deletion] was identified in 31 of 887 (3.5%) of NDMM and 18 of 121 (15%) of RMM, where biallelic deletion predominates (12%; Fig. 2B). CoMMpass analysis also identified copy-number–dependent expression of *RB1* (median $log_2$ TPM levels for 0, 1, 2, and 3 or more copies of 1.83, 4.62, 5.41, and 6.26, respectively, with high significance according to Jonckheere–Terpstrata nonparametric trend test; Fig. 2C) with infrequent biallelic inactivation associated with poor prognosis (Fig. 2D), matching results from FoundationOne panel data (19).

## *Rb1* Haploinsufficiency Does Not Contribute to Myeloma Progression

The prevalence of monosomy 14 in Vk*MYC mice, coupled with *Rb1* biallelic deletions (Fig. 1B), prompted us to investigate the contribution of *Rb1* loss to multiple myeloma progression in Vk*MYC mice. Because the Vk*MYC mice carry LoxP sites flanking the transgenic 3′ *kappa* enhancer responsible for driving *MYC* expression in PCs (Supplementary Fig. S2), any genetic cross with mice expressing CRE recombinase in B cells will cause floxing of the transgene and suppression of *MYC* transcription. We therefore crossed Vk*MYC mice with constitutive $Rb1^{het}$ mice to generate multiple myeloma tumors lacking one copy of *Rb1*. Constitutive *Rb1* biallelic loss is embryonic lethal, and $Rb1^{het}$ mice have been shown to develop pituitary tumors in which the remaining copy of *Rb1* is lost (20). Consistently, we observed a shorter overall survival (OS) in $Rb1^{het}$ mice (median OS, 57 weeks) compared with wild-type (WT) mice (120 weeks). Loss of one *Rb1* copy also significantly reduced the OS of Vk*MYC mice (83 weeks for Vk*MYC vs. 67 weeks for Vk*MYCx$Rb1^{het}$ mice; Fig. 2E). Similar to $Rb1^{het}$ mice, the early mortality noted in Vk*MYCx$Rb1^{het}$ mice was attributable to the development of pituitary tumors and not to the acceleration of multiple myeloma progression. We previously reported that multiple myeloma cells in Vk*MYC mice secrete a large amount of monoclonal immunoglobulin detectable by serum protein electrophoresis (SPEP) as M-spikes, which are a clinically useful marker for tumor burden (2). We therefore compared the incidence of M-spike development between Vk*MYC and Vk*MYCx$Rb1^{het}$ mice by serial SPEP analysis conducted over time in cohorts of mice across genotypes. Loss of one copy of *Rb1* did not accelerate the development of monoclonal gammopathy in Vk*MYC mice. Similarly, no differences were noted in the incidence of M-spike between WT and $Rb^{het}$ mice (Fig. 2F). In an attempt to isolate the multiple

**Table 1. Tabulation of recurrent CNAs observed in Vk*MYC tumors**

| Sample | Origin | Sex | Trisomy | Monosomy | Sex chr. loss | Biallelic deletions |
|---|---|---|---|---|---|---|
| Vk12598 | Transplant | M | 15,17 | | Y | *Kdm6a* |
| Vk12653 | Transplant | M | | 5,8,14 | Y | *Cdkn2a, Kdm6a, Rb1* |
| Vk12728 | *De novo* | F | | | | |
| Vk12803 | *De novo* | F | 9 | | X | |
| Vk12811 | *De novo* | F | | | X | *Kdm6a* |
| V12869 | Transplant | M | 1 | | Y | *Rb1* (1N) |
| V12996 | *De novo* | M | | | | |
| Vk13044 | Transplant | F | | | X | |
| Vk13045 | Transplant | F | | 5,14 | X | *Kdm6a* |
| Vk13051 | Transplant | F | 1,16 | | X | |
| Vk13321 | Transplant | M | | 5 | | *Rb1, Mir15a/Mir16-1* (1N) |
| VK13410 | *De novo* | F | | | | |
| Vk13429 | *De novo* | M | 19 | 5,14 | Y | *Rb1* |
| Vk13742 | *De novo* | F | | 5,14 | | |
| Vk13756 | *De novo* | M | | 5,14 | Y | *Kdm6a* |
| V13769 | *De novo* | M | | 5 | | |
| Vk13795 | *De novo* | M | 1 | 5 | | |
| V13801 | *De novo* | F | 6 | | | |
| V13826 | *De novo* | F | 18 | 5,14 | X | |
| Vk13855 | *De novo* | F | 6,16 | | X | |
| Vk14123 | Transplant | F | 6 | | X | |
| V14153 | *De novo* | M | 18 | 5 | Y | *Kdm6a* |
| V14154 | Transplant | F | | | | *Cdkn2a* |
| V14246 | *De novo* | M | | 5 | | |
| Vk14660 | *De novo* | F | | 5 | X | *Kdm6a* |
| Vk15051 | *De novo* | M | | 5 | Y | |

myeloma phenotype and propagate multiple myeloma cells, we transplanted BM mononuclear cells isolated from moribund Vk*MYCx*Rb1*$^{het}$ mice into WT recipient mice and monitored them by SPEP. No M-spike was detected up to 1 year after transplantation, indicating that tumor engraftment did not occur (Supplementary Fig. S3A). This was likely due to the low tumor burden of the donor mice (average BM PC content was 5.79%), which were euthanized before aggressive multiple myeloma had developed. In a retrospective analysis of Vk*MYC tumor transplantation, we observed that successful multiple myeloma engraftment into recipient mice is more likely to occur when donor organs (either spleen, BM, or lymph nodes) have higher PC content (mean PC is 13.1% for nonengrafted and 28.2% for engrafted tumors; Supplementary Fig. S3A). Significantly, the odds of engraftment for donor tumor PC content >10% were over seven times greater than for cases with donor tumor PC content <10% [OR 7.79 (1.69–35.92); Fisher $P < 0.01$]. On the other hand, the age of the donor mouse did not affect the ability of the tumor to engraft, although Vk*MYCx*Rb1*$^{het}$ donors were significantly younger than the Vk*MYC donors in our analysis (Supplementary Fig. S3B). We therefore conclude that loss of one *Rb1* copy does not contribute to multiple myeloma initiation or progression. However, the presence of focal *Rb1* biallelic deletions observed in multiple myeloma tumors from Vk*MYC mice, as well as in human multiple myeloma, clearly indicates that complete *Rb1* inactivation is selected by multiple myeloma cells and likely plays a role in tumor progression.

## Monoallelic Loss of *Mir15a/Mir16-1* Accelerates Monoclonal Gammopathy in Wild-Type C57BL/6 Mice

Having excluded *RB1* as a key gene driving chromosome 13 loss in multiple myeloma, we investigated the contribution of *MIR15A/MIR16-1* haploinsufficiency to multiple myeloma initiation and progression. The generation of mice carrying germline or conditional deletion of either the CLL chromosome 13 MDR, containing the *Mir15a/Mir16-1* cluster and the *DLeu2* gene (hereinafter referred to as MDR mice) or the *Mir15a/Mir16-1* cluster alone (referred to as MIR mice) has been described, where MIR and MDR mice develop B-cell–autonomous clonal lymphoproliferative conditions

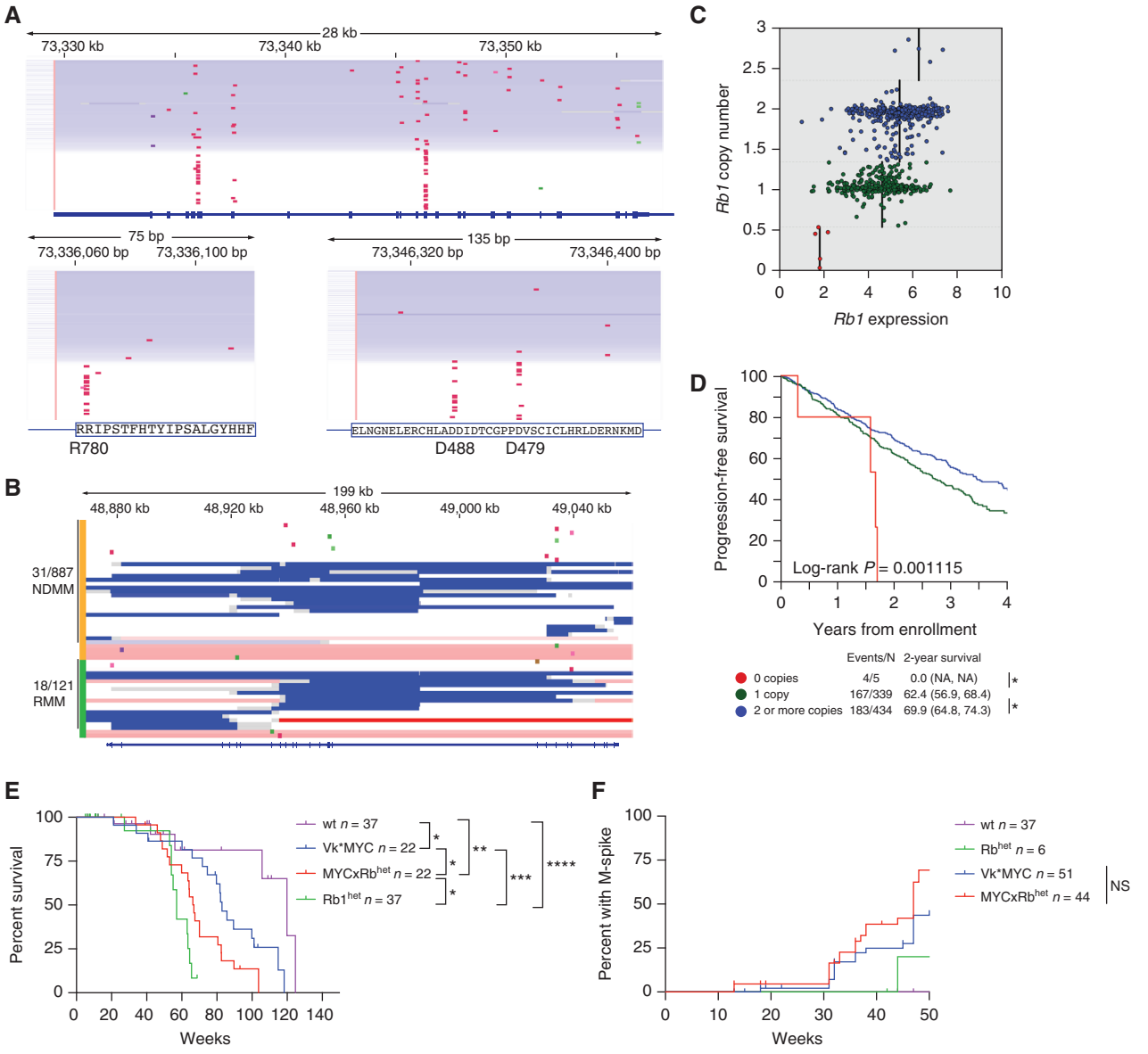


**Figure 2.** *Rb1* haploinsufficiency does not contribute to multiple myeloma initiation and progression. **A,** Copy-number abnormalities and NS-SNV are shown for 91 NDMM with *DIS3* mutations. Top, the complete 28kb *DIS3* genomic locus; bottom, codons R780, D488, and D479. The patients are ordered vertically by degree of copy loss, with light blue indicating one copy loss, and white no copy loss; 101 missense SNVs are colored red, 2 splice-donor site SNVs purple, 2 splice-acceptor site SNVs light green, and 3 start-loss SNVs dark green. **B,** *RB1* CNA and NS-SNV are shown for 35 NDMM (orange bar) and 20 RMM (green bar), the color scale accentuates biallelic deletion in dark blue [$\log_2(CN/2) \leq 1.5$], one copy loss in white [$-1.5 < \log_2(CN/2) \leq 0.5$], and no copy loss in pink and red [$\log_2(CN/2) > -0.5$]. *RB1* is biallelically inactivated in 31 of 924 NDMM (10 NS-SNV associated with LOH, and 21 with biallelic deletion), and in 18 of 121 RMM (3 NS-SNV associated with LOH, and 15 with biallelic deletion); 8 stop-gain SNV are colored red, 2 frameshift SNV light green, 4 missense SNV dark green, 4 splice-donor SNV pink, and 1 splice acceptor SNV brown. **C,** Visualization of copynumber-dependent expression of *RB1* ($\log_2$ TPM) in patients with newly diagnosed multiple myeloma enrolled in the CoMMpass clinical study. Vertical lines indicate median *RB1* expression for a given copy number level. **D,** PFS of patients with newly diagnosed multiple myeloma enrolled in the CoMMpass clinical study sorted by *RB1* copy number (overall log-rank $P < 0.001$). **E,** OS in weeks of mice of the indicated genotype (*n* indicates number of mice analyzed for each group). **F,** Incidence of M-spike for the same mice as in **C**, detected by serum protein electrophoresis performed at the indicated week. *n* indicates number of sera analyzed for each group. For **E** and **F,** *P* values for log-rank (Mantel–Cox) test are shown with *, $P < 0.05$; **, $P < 0.01$; ***, $P < 0.001$; ****, $P < 0.0001$; NS, nonsignificant.

with shorter OS for MDR$^{null}$ mice only (15). We aged a cohort of littermate WT, MDR$^{het}$, and MDR$^{null}$ mice and analyzed them by SPEP, performed every 10 weeks, for evidence of monoclonal gammopathy. C57BL/6 WT mice, known to spontaneously develop a gammopathy with age (21), had a median time to develop an M-spike (time to spike, TTS) of 96 weeks (Fig. 3A). Loss of one copy of *Mir15a/Mir16-1* cluster in MDR$^{het}$ mice significantly accelerated M-spike development, reducing the TTS to 57 weeks, while complete *Mir15a/Mir16-1* loss in MDR$^{null}$ mice further reduced the TTS to 48 weeks. Notably, the intensity of the observed M-spikes remained stable over time in all the cohorts analyzed, with a gamma/

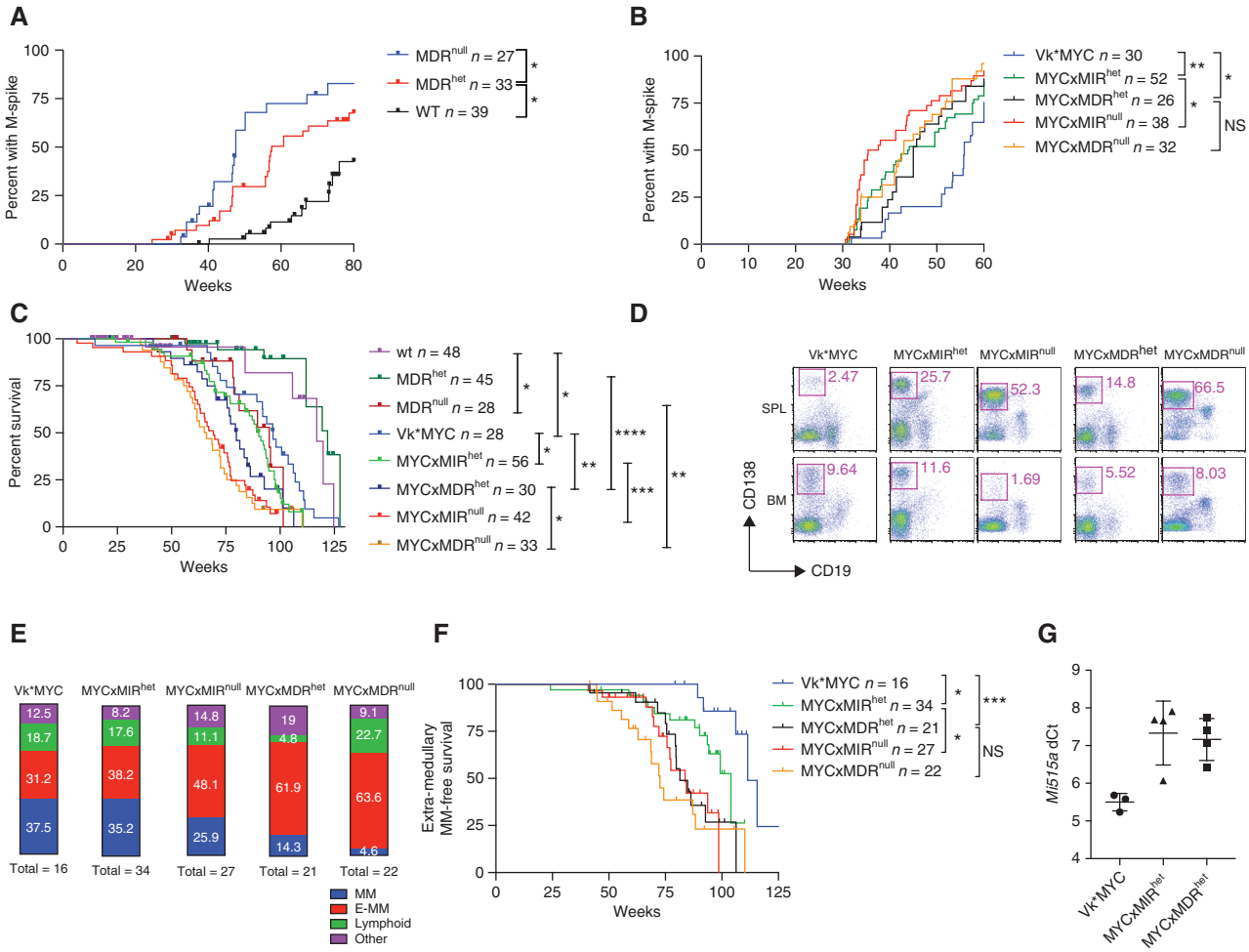


**Figure 3.** Loss of one copy of the *Mir15a/Mir16-1* cluster accelerates M-spike development and promotes multiple myeloma progression and extramedullary dissemination. Incidence of M-spikes over time (weeks) in cohorts of WT, MDR$^{het}$, or MDR$^{null}$ littermate mice (**A**) or in Vk*MYC mice alone or crossed with mice lacking one or two copies of the *Mir15a/Mir16-1* cluster only (MYCxMIR) or both the *dLeu2* gene and the *Mir15a/Mir16-1* cluster (MYCxMDR; **B**). *n* indicates number of sera for each group analyzed by serum protein electrophoresis at the indicated week. **C,** Kaplan–Meier overall survival plot in weeks for the same cohort of mice as in **B**. *n* indicates number of mice in each group. **D,** Representative flow cytometric analysis performed on spleen and BM cells collected from moribund mice of the indicated genotype. Numbers indicate the percentage of plasma cells (CD19$^-$CD138$^+$) within the pink gates. **E,** Incidence of multiple myeloma (MM), extra-medullary multiple myeloma (E-MM), lymphoproliferative disease (Lymphoid), and other conditions (Other) detected by flow cytometric analysis performed at necropsy on moribund mice of the indicated genotype. Numbers within each box indicate the percentage of each condition, and the total number of necropsied mice is shown. **F,** Extra-medullary multiple myeloma–free survival (in weeks) for the same cohorts of mice as in **C**. *n* indicates number of mice in each group. **G,** *miR-15a* expression evaluated by qPCR (TaqMan assay) in multiple myeloma tumors harvested from Vk*MYC, MYCxMIR$^{het}$, or MYCxMDR$^{het}$ mice. $\Delta C_t$ (threshold cycle) values were normalized to U6 RNA. Each dot represents the average value from an individual tumor assayed in triplicate. Lines indicate mean with SD. *P* values for log-rank (Mantel–Cox) test are shown, with *, $P < 0.05$; **, $P < 0.01$; ***, $P < 0.001$; ****, $P < 0.0001$.

albumin ratio ≦ 0.1 indicating that losing one copy of *Mir15a/Mir16-1* promotes clonal PC accumulation in WT mice, but it is not sufficient to drive its malignant transformation to multiple myeloma.

## Monoallelic Loss of *Mir15a/Mir16-1* Accelerates Myeloma Progression in Vk*MYC Mice

Having observed a role for *Mir15a/Mir16-1* haploinsufficiency in PC expansion, we crossed both MIR and MDR constitutive mice with Vk*MYC mice and monitored them over time for multiple myeloma development and progression. Vk*MYC mice, as reported previously, developed M-spikes beginning at 30 weeks of age, with 50% of the mice having a detectable M-spike by 56 weeks (2). Biallelic loss of the *miR15-a/16-1* cluster significantly accelerated the TTS, with 50% of Vk*MYCxMIR$^{null}$ and Vk*MYCxMDR$^{null}$ mice developing M-spikes at 36 and 43 weeks, respectively. An acceleration in M-spike development was evident even in mice with one copy of *Mir15a/Mir16-1*, with 50% of Vk*MYCxMIR$^{het}$ and Vk*MYCxMDR$^{het}$ mice developing M-spikes at 44 and 45 weeks, respectively (Fig. 3B).

Consistent with the increase in tumor burden, the copy number level of *Mir15a/Mir16-1* also had a significant effect on the OS of the mice. As previously reported, loss of one

copy of the MDR region did not reduce the OS of WT mice, while biallelic loss did (117 vs. 95 weeks; ref. 15). The 97-week median survival observed for the Vk*MYC mice was reduced to 90 and 68 weeks by the loss of one or two copies of the *Mir15a/Mir16-1* cluster, respectively, or to 80 and 66 weeks by the loss of one or two copies of the MDR region (which includes *DLeu2*; Fig. 3C). Flow cytometric and histologic analysis performed at necropsy identified the presence of extra-medullary (E-MM) PC expansion, defined by the presence of more than 8% PC in extra-medullary sites (most commonly spleen and mesenteric lymph nodes), in Vk*MYC mice with monoallelic or biallelic *Mir15a/Mir16-1* deletion, with increased frequency in the latter (Fig. 3D and E). Overall, loss of *Mir15a/Mir16-1* did not alter the nature of MYC driven PC dyscrasia and expansion of monoclonal $CD19^-$ $CD138^+$ PCs occurring with an approximated incidence of 70% across all the genotypes analyzed. However, loss of *Mir15a/Mir16-1* accelerated its manifestation and promoted extra-medullary disease dissemination in a dose-dependent manner. Consistently, the E-multiple myeloma–free survival was significantly shorter in mice lacking one or two copies of the *Mir15a/Mir16-1* cluster compared with Vk*MYC mice (Fig. 3F).

Next, we wondered whether multiple myeloma tumors that arose in Vk*MYCxMIR$^{het}$ and Vk*MYCxMDR$^{het}$ mice had retained the second copy of the *Mir15a/Mir16-1* cluster or had acquired *Mir15a/Mir16-1* complete inactivation. We employed a TaqMan qPCR assay and measured *Mir15a* expression in total RNA isolated from $CD138^+$ multiple myeloma cells. $\Delta C_t$ values normalized against U6 snRNA indicated a maintained expression of *Mir15a* in the heterozygous tumors with decreased expression levels compared with Vk*MYC tumors with two copies of *Mir15a* (Fig. 3G). As expected, no *Mir15a* expression was detected in tumors from Vk*MYCxMIR$^{null}$ and Vk*MYCxMDR$^{null}$ mice. We concluded that *Mir15a/Mir16-1* haploinsufficiency accelerates multiple myeloma development in Vk*MYC mice.

It was previously noted that mice carrying constitutive or B-cell–specific loss of *Mir15a/Mir16-1* cluster had an identical B-cell-autonomous–driven phenotype (15). Because we were not able to evaluate conditional *Mir15a/Mir16-1* deletion in Vk*MYC mice, we wondered whether reduced *Mir15a/Mir16-1* expression in the multiple myeloma microenvironment could contribute to the phenotype we observed. Specifically, it has been reported that multiple myeloma cell lines cocultured with BM mesenchymal cells derived from MIR$^{null}$, but not WT mice, display higher proliferation rates (22) and that Mir16 levels regulate the polarization state of tumor-promoting M2 macrophages (23, 24). We therefore compared engraftment rate in WT, MDR$^{het}$, and MDR$^{null}$ littermate recipient mice transplanted with Vk12598 multiple myeloma tumors lacking del(14), and found no differences in the time of appearance of M-spikes and their progression over time among the three cohorts analyzed (Supplementary Fig. S4A), although MDR$^{null}$ recipients had shorter OS (43.5 days compared with 53 days for MDR$^{het}$ and 55 days for WT recipients; Supplementary Fig. S4B). We therefore concluded that although complete loss of *Mir15a/Mir16-1* in the tumor microenvironment may favor myelomagenesis, *Mir15a/Mir16-1* haploinsufficiency has a clear tumor cell–autonomous role in promoting multiple myeloma progression. Overall, these data indicate that *Mir15a/Mir16-1* regulates multiple myeloma initiation and progression in a copy number–dependent way, with a more aggressive tumor course in mice lacking both copies of the *Mir15a/Mir16-1* cluster.

## Loss of the *Mir15a/Mir16-1* Cluster Induces Myeloma Cell Proliferation in Vk*MYC Mice

Next, we sought to characterize the effects of *Mir15a/Mir16-1* deletion at the molecular level in multiple myeloma and compared gene expression profile (Affymetrix) in $CD138^+$ PCs harvested from 45 independent Vk*MYC mice with multiple myeloma (*de novo*), 16 Vk*MYC tumor–bearing mice (transplants), 18 Vk*MYCxMIR$^{null}$ and Vk*MYCxMDR$^{null}$ *de novo* mice (MIR), and 5 age-matched WT controls (normal PC from BM and spleen). As a reference, we also included in our analysis two Balb/c plasmacytoma (PCT) cell lines (XRPC24 and LS136) and four Burkitt's lymphoma tumors that arose spontaneously in Vk*MYC mice in our analysis (2). Principal component analysis of differentially expressed genes clearly clustered the samples based on their cell of origin (B cell vs. PC), with the Burkitt's lymphoma samples more spatially separated and normal PCs (NPC) and PCT samples distinct from Vk*MYC–derived multiple myeloma samples, which clustered closer together (Fig. 4A). Consistently, the expression of PC (*Irf4, Sdc1, Xbp1, Prdm1, Tnfrsf17*) versus B-cell (*Pax5, Cd19, Cd79b*) lineage–specific genes underscored the terminally differentiated status of Vk*MYC and Vk*MYCxMIR multiple myeloma tumors (Fig. 4B). Analysis of differentially expressed genes in multiple myeloma cells from *de novo* mice lacking one or two copies of the *Mir15a/Mir16-1* cluster, Vk*MYCxMIR, and Vk*MYCxMDR, compared with Vk*MYC mice with two copies of *Mir15a/Mir16-1,* identified cell-cycle genes previously reported to be direct *Mir15a/Mir16-1* targets in CLL and multiple myeloma (Fig. 4C; Supplementary Table S1; refs. 15, 17, 25). Genes upregulated in Vk*MYCxMIR and Vk*MYCxMDR mice include *Chek1, Chek2, Mcm5, Mcm10, Cdk4*, and *Cse1l/Xpo2*, along with *Mcm2* and *Mcm7, Ccnb1, Ccna2, Birc5*, and *Cdkn2a*. In addition, the origin recognition complex genes *Orc5* and *Orc2*, which are essential for initiation of DNA replication and recruitment of MCM proteins that form the DNA helicase complex, and the melanoma-associated antigen, *Magea4*, shown to abrogate p53 induced cell-cycle arrest (26), were also upregulated in MIR and MDR mice tumors. Consistently, gene set enrichment analysis identified significant enrichment in additional genes in the cell-cycle and DNA replication pathways (Supplementary Fig. S5A and S5B). Unexpectedly, pathway analysis also identified upregulation of genes involved in RNA transport and protein translation initiation, including the Ras-related nuclear protein, *Ran*; the exportins *Xpo1/Crm1* and *Xpot*, which shuttle RNAs and ribosomal subunits from the nucleus to the cytoplasm, hydrolize GTP, and return to the nucleus (27, 28); the mRNA export factor *Rae1* and several genes encoding for the nuclear pore complex, previously implicated in tumorigenesis (29); the protein arginine methyltransferases *Prmt5* and two members of the SMN complex *Ddx20/Gemin3*; *Gemin5* required for correct assembly of the spliceosome (30); and several subunits of eukaryotic initiation factors eIF3, which control translation of cell proliferation mRNAs (31), for example, eIF5, eIF1, and

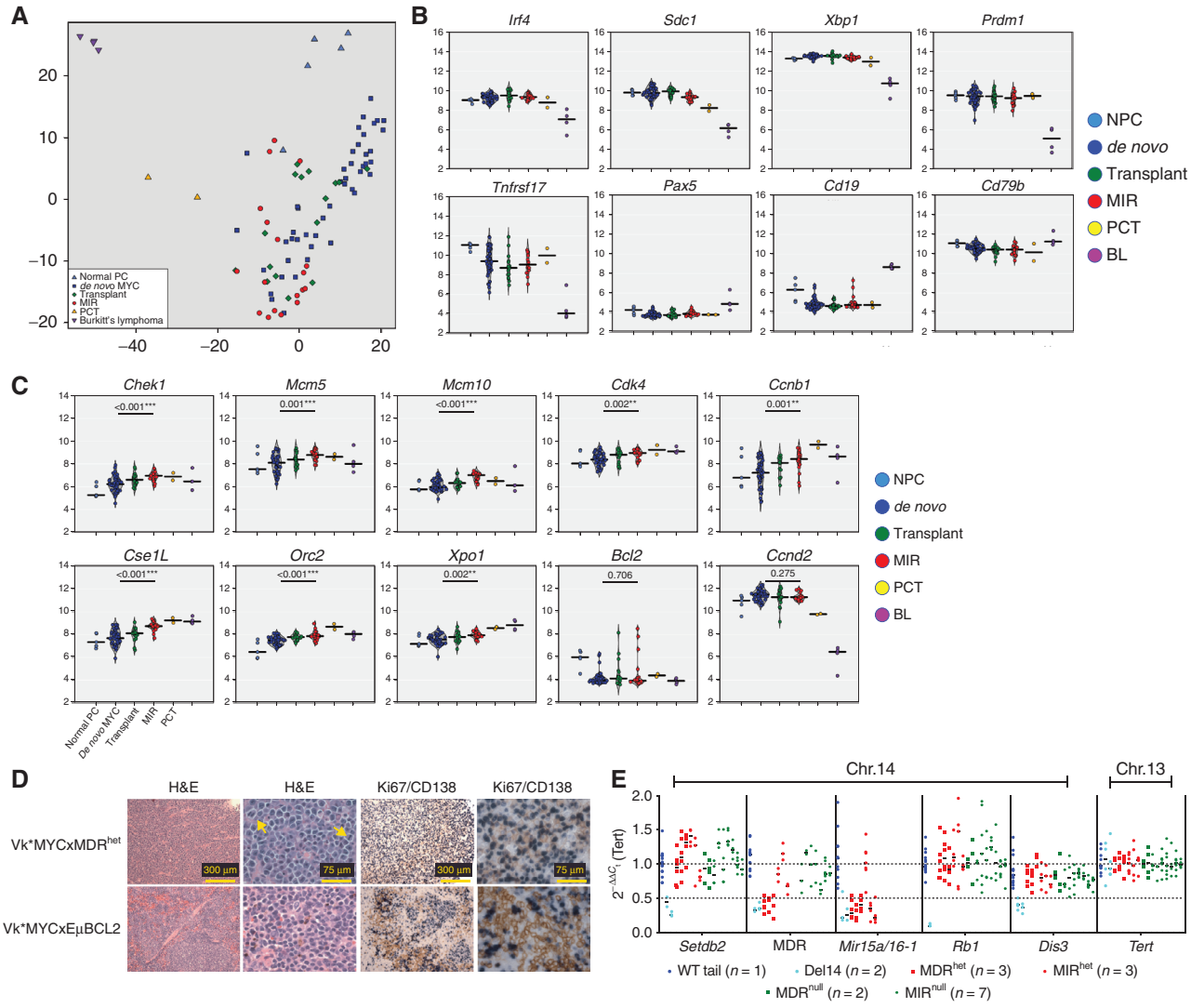


**Figure 4.** Loss of one copy of the *Mir15a/Mir16-1* cluster promotes multiple myeloma cell proliferation. Visualization of the two most variable principle components from the top 5,000 most variable genes (**A**) and differential expression of plasma cells and B-cell lineage–specific genes (**B**) or cell-cycle genes (**C**), in NPCs from aged WT mice, *de novo*, or transplant Vk*MYC mice alone or crossed with mice lacking one or two copies of the *Mir15a/Mir16-1* cluster only or of both the *dLeu2* gene and the *Mir15a/Mir16-1* cluster, all grouped together (MIR), Balb/c plasmacytoma lines (PCT) or Vk*MYC derived Burkitt's lymphoma tumors (BL). *P* values comparing *de novo* Vk*MYC to MIR mice are indicated. **D,** Assessment of proliferation by ki67 staining (blue) in formalin-fixed, paraffin-embedded tumor tissues from representative Vk*MYCxMDR$^{het}$ or Vk*MYCxEμBCL2 mice. Magnification bars are shown. **E,** qPCR analysis performed on genomic DNA from WT, Vk*MYC, Vk*MYCxMIR, or Vk*MYCxMDR mice. $\Delta C_t$ values for the indicated genes, displayed in their genomic order on chromosome 14, were normalized to *Tert* as a diploid control. Each dot represents the calculated $2^{-\Delta\Delta C_t}$ gene levels from an individual tumor assayed in triplicate. The number of independent tumors analyzed for each genotype is indicated. The dotted horizontal lines mark haploid and diploid gene levels.

eIF2b (Supplementary Fig. S6). *Bcl2, Vegfa, Tab3*, and *Cabin1*, previously reported to be direct *miR15-a/16-1* targets in multiple myeloma or CLL, were not differentially expressed in MYCxMIR tumors (17, 32–34). However, *Bcl2* was not generally expressed in Vk*MYC tumors, with appreciable expression in 3 of 45 *de novo* Vk*MYC compared with 3 of 16 transplant and 3 of 18 Vk*MYCxMIR and Vk*MYCxMDR tumors, where the expression levels were 2- to 4-fold higher. In addition, we did not observe significant upregulation of *Ccnd1, -2*, or *-3* in Vk*MYCxMIR and Vk*MYCxMDR tumors, above the high levels of *Ccnd2* found in all Vk*MYC tumors (mean $\log_2$ RMA-normalized *Ccnd2* levels = 11.402; Fig. 4C). Surprisingly, we observed high levels of *Ccnd2* also in five NPCs harvested from aged C57BL/6 WT mice (= 10.783), which were not seen in four Burkitt's lymphoma tumors that spontaneously developed in Vk*MYC mice (= 6.180; ref. 2).

Overall, the pattern of gene expression found in NPC, multiple myeloma samples harvested from *de novo* Vk*MYC, or from transplant Vk*MYC mice demonstrated an increasingly more proliferative disease, at least in part, supported by *Cdkn2a* biallelic inactivation found in transplant, but not *de novo* Vk*MYC tumors (Table 1), and consistent with the previously reported more aggressive and drug-resistant nature of the transplanted model (6). Interestingly, *de novo*

**Table 2. Frequency of del(13q) by FISH analysis in molecular subtypes of MGUS and multiple myeloma**

| Genetic classification | Total | | % Total | | % excluding insuff PC | | % ≥1 FISH abnl | | Del13/13q Present | | % del13 | | Fisher test |
|---|---|---|---|---|---|---|---|---|---|---|---|---|---|
| | MGUS | MM | MGUS | MM | MGUS | MM | MGUS | MM | MGUS | MM | MGUS | MM | *P* |
| Insufficient PC | 107 | 190 | 28% | 10% | | | | | | | | | |
| No FISH abnormality | 72 | 118 | 19% | 6% | 26% | 7% | | | | | | | |
| CCND: t(11;14) or t(6;14) | 64 | 341 | 17% | 18% | 23% | 20% | 32% | 21% | 13 | 125 | 20% | 37% | 0.014 |
| MMSET: t(4;14) | 8 | 155 | 2% | 8% | 3% | 9% | 4% | 10% | 6 | 127 | 75% | 82% | 0.640 |
| MAF: t(14;16) or t(14;20) | 16 | 75 | 4% | 4% | 6% | 4% | 8% | 5% | 6 | 57 | 38% | 76% | 0.005 |
| HRD11$^{+}$ | 43 | 444 | 11% | 23% | 16% | 26% | 21% | 28% | 7 | 86 | 16% | 19% | 0.839 |
| HRD11$^{-}$ | 13 | 217 | 3% | 11% | 5% | 13% | 6% | 14% | 9 | 107 | 69% | 49% | 0.253 |
| nHRD2 | 59 | 359 | 15% | 19% | 21% | 21% | 29% | 23% | 36 | 219 | 61% | 61% | 1.000 |
| Total | 382 | 1899 | 382 | 1899 | 275 | 1709 | 203 | 1591 | 77 | 721 | 38% | 45% | 0.051 |

Note: Patients assigned to mutually exclusive groups, starting from the top, after excluding those with insufficient PCs or with no FISH abnormalities. Seventeen patients had a report of hyperdiploidy alone without mention of specific chromosomes and were excluded from the analysis. HRD11$^{+}$: 11+ and at one of 3+,7+,9+,15+. nHRD2, the remaining patients (no recurrent translocation or hyperdiploidy).
Abbreviation: MM, multiple myeloma.

Vk*MYCxMIR and Vk*MYCxMDR tumors displayed even higher levels of proliferation markers. Histologic examination of spleen sections collected from Vk*MYCxMIR and Vk*MYCxMDR mice with multiple myeloma and stained with hematoxylin and eosin revealed the presence of characteristic mitotic figures, absent in control spleen sections from age-matched Vk*MYC mice or even Vk*MYC crossed with Eμ-BCL2 mice (Vk*MYCxEμ-BCL2), chosen as a control for extra-medullary multiple myeloma (2). Furthermore, double staining with antibodies against CD138, which identifies PCs, and Ki67, a marker of cell proliferation, identified cycling multiple myeloma cells in the spleen of Vk*MYCxMIR or Vk*MYCxMDR mice, but not Vk*MYCxEμ-BCL2 mice (Fig. 4D).

## Vk*MYC Tumors with Mono or Biallelic Loss of *Mir15a/Mir16-1* Cluster Do Not Acquire Monosomy 14

Subsequently, we considered whether multiple myeloma tumors harvested from Vk*MYCxMIR and Vk*MYCxMDR mice developed del(14) with the same frequency as Vk*MYC mice. We designed and validated qPCR primer sets against genes distributed along chromosome 14 (*Setdb2, Rb1, Dis3*, as well as *Mir15a/Mir16-1* and MDR) and included *Tert* as a normalizer diploid locus. The qPCR analysis correctly identified monosomies of chromosome 14 tested in two multiple myeloma tumors with known del(14) detected by aCGH, but not in WT genomic DNA (Fig. 4E). The assay also confirmed monosomic *Mir15a/Mir16-1* and MDR loci in multiple myeloma tumors from Vk*MYCxMIR$^{het}$ ($n = 3$) and Vk*MYCxMDR$^{het}$ ($n = 3$) mice. However, no other regions of chromosome 14 loss were identified in any of the multiple myeloma tumors from Vk*MYCxMIR ($n = 10$) or Vk*MYCxMDR ($n = 5$) mice. Similarly, no NS-SNV were identified in targeted sequence analysis of *Rb1, Dis3*, or *Mir15a/Mir16-1*.

## Deletion of *MIR15A/MIR16-1* Is Present in MGUS Patients

Having identified a role for reduced *Mir15a/Mir16-1* expression in monosomy 14 associated with increased multiple myeloma cell proliferation and disease progression in mice, we sought to investigate the frequency of monosomy 13 in the major molecular subtypes of MGUS and multiple myeloma. In an analysis of patients treated or observed at Mayo Clinic, patients were first classified into six distinct molecular groups based on the presence of a recurrent IgH translocation [CCND: t(11;14) and t(6;14); MAF: t(14;16) and t(14;20); MMSET: t(4;14)], or hyperdiploidy, divided into two main types based on the presence of trisomy 11 [unsupervised hierarchical clustering of copy number abnormalities in multiple myeloma by Walker and colleagues (9) identified cluster 1 (HRD11–) vs. cluster 2 (HRD11+)], with the remaining patients without hyperdiploidy or recurrent IgH translocations classified as nonhyperdiploid (nHRD2). FISH was performed on 382 patients with MGUS and 1,899 with multiple myeloma (11, 35). Similar to previous analyses (10, 11), there was a marked difference in the frequency of del(13), identified by loss of an *RB1* probe, based on the molecular groups, with the lowest frequency (19%) in HRD11$^{+}$ and highest (80%) in the MMSET and MAF groups (Table 2). Within each molecular group, the frequency of del(13) was similar in MGUS versus multiple myeloma, with the exception of the CCND (20% vs. 37%) and MAF (38% vs. 76%) groups where del(13) is clearly associated with progression from MGUS to multiple myeloma. We concluded that del(13) occurs at a very early stage in the pathogenesis of multiple myeloma and

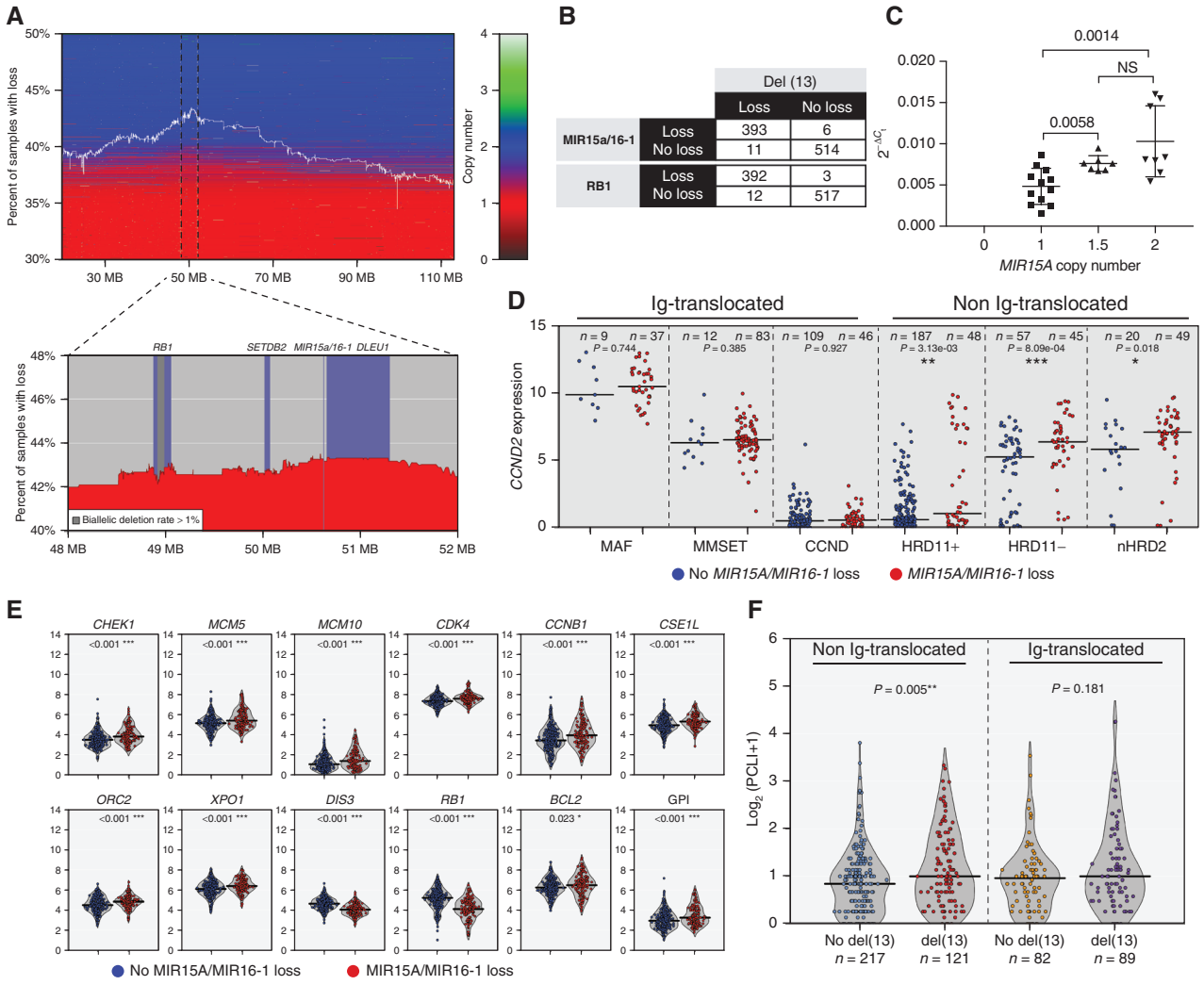


**Figure 5.** *MIR15A/MIR16-1* monosomy is associated with increased proliferation in non-Ig-translocated NDMM. **A,** Investigation of CoMMpass NDMM copy number levels of chromosome 13 show region surrounding *MIR15A/MIR16-1* to be the most frequently lost. The white line indicates the percentage of all cases with a loss at specific locations along chromosome 13 where horizontal shading reproduces segmentation data for each patient sorted vertically according to the percentage of total loss of chromosome 13. **B,** Distribution of NDMM cases with or without copy number loss of *MIR15A/16-1* or *RB1* relative to presence or absence of del(13). **C,** Relative expression of MIR15a (normalized to *U6* snRNA) in multiple myeloma cell lines relative to *MIR15A* copy number. Each dot represents the average *MIR15A* value calculated by TaqMan assay using the $2^{-\Delta C_t}$ method from triplicate assays for each cell line tested. *P* values for nonparametric *t* test are shown. **D,** $Log_2$-transformed TPM data for NDMM reveal increased *CCND2* expression in non-Ig-translocated cases with loss of *MIR15A/MIR16-1*. **E,** Increased expression of proliferation targets (*CHEK1, MCM5, MCM10, CDK4*, and *CCNB1*), DNA replication (*ORC2*), nuclear transport (*XPO1* and *CSE1L*), and antiapoptotic (*BCL2*) genes for NDMM non-Ig-translocated cases with loss of *MIR15A/MIR16-1*, resulting in overall increase in GPI. In addition, expression of markers on chromosome 13 (*DIS3, RB1*) shows copy number dependency. The number of patients within each group and Wilcoxon *P* values for each comparison are shown for **D** and **E**. **F,** Plasma cell labeling index calculated by flow cytometry in clonal PCs collected at the time of diagnosis in the indicated subgroups, divided into Ig-translocated and not translocated, with or without del(13) according to FISH analysis. The number of patients within each group and Wilcoxon *P* values for each comparison are shown.

loss of one copy of *MIR15a/MIR16-1* is likely to contribute to the immortalization of the MGUS clone, as we noted in mice with one copy of *Mir15a/Mir16-1*, which displayed an increased incidence in monoclonal gammopathy (Fig. 3A).

## Deletion of *MIR15A/MIR16-1* Is Associated with Increased Proliferation in Patients with Multiple Myeloma

The analysis of copy number changes in the IA14 CoMMpass dataset found evidence of del(13), defined by a mono or biallelic loss of more than 10% of the length of chromosome 13, in 44% of 924 NDMM, with a newly identified peak region of deletion occurring around *MIR15A/MIR16-1* (Fig. 5A). While most of the samples with loss of *MIR15A/MIR16-1* or *RB1* also have del(13), 6/399 and 3/395 samples, respectively, showed specific copy number loss of *MIR15A/MIR16-1* or *RB1* without del(13) (Fig. 5B). Having identified copy number dependent expression of *MIR15A* in a panel of multiple myeloma cell lines (Fig. 5C), we decided to compare gene expression in patients with multiple myeloma with and without *MIR15A/MIR16-1* loss. The most

striking difference we noted was the increased expression of *CCND2* associated with *MIR15A/MIR16-1* loss (Supplementary Fig. S7A). However, we reasoned that this observation could simply be a reflection of the fact that del(13) multiple myeloma cases are enriched by those belonging to the MAF or MMSET groups (78% of MAF, 88% of MMSET), which have a unique transcriptional profile characterized by increased *CCND2* expression (36). Furthermore, other multiple myeloma cases carry IgH chromosome translocations directly dysregulating D-type cyclins, known *MIR15A/MIR16-1* target genes. To isolate the transcriptional effects associated to *MIR15A/MIR16-1* loss, we therefore restricted our analysis to the remaining 58% CoMMpass cases, altogether defined as non-Ig translocated and comprising HRD11$^{+}$, HRD11$^{-}$, and nHRD2 groups. Even in this controlled analysis, we observed significantly higher *CCND2* expression associated to *MIR15A/MIR16-1* loss in the non-Ig–translocated group (Fig. 5D). When we looked at the expression of other *MIR15A/MIR16-1* target genes in the same group of patients, we found that *MIR15A/MIR16-1* loss was strikingly associated with increased expression of the exact same proliferation and nuclear transport markers we identified in Vk*MYCxMIR and Vk*MYCxMDR mice with copy number loss of *Mir15a/Mir16-1* (Figs. 4C and 5E). Overall, the upregulation of cell-cycle genes resulted in a marked increase in the gene proliferation index (GPI), as defined previously (ref. 37; Fig. 5E). In contrast, with the exception of *CDK4*, no difference in expression of *MIR15A/MIR16-1* target genes was observed in NDMM cases with Ig translocations (Supplementary Figs. S5D and S7B). Finally, in an independent cohort of 612 multiple myeloma patients treated at the Mayo Clinic with available FISH and PC labeling index (PCLI) data collected one month before or within 6 months from initial diagnosis, we identified a significant association between presence of del(13) and increased PCLI for the non-Ig-translocated group (Fig. 5F). We therefore concluded that aberrations to chromosome 13 provide significant positive contribution to proliferation in patients with multiple myeloma lacking Ig translocation.

## DISCUSSION

Genomics analysis of multiple myeloma tumors harvested from Vk*MYC mice showed similarity with human multiple myeloma. Like human multiple myeloma, Vk*MYC multiple myeloma tumors express canonical markers of PC terminal differentiation, including *Sdc1, Irf4, Xbp1, Prdm1,* and *Tnfrsf17* (*Bcma*), and lack expression of B-cell markers like *Cd19* and *Pax5*. As we have identified universal CCND dysregulation in human multiple myeloma tumors (36), we found that Vk*MYC multiple myeloma also display high levels of *Ccnd2* expression. Among other genomic changes reported in human multiple myeloma, albeit at low frequency, we identified inactivation of *Rb1* in three, *Cdkn2a* (p16/ARF) in two and of *Kdm6a/Utx* in seven of 26 tumors. While deletion of *RB1* and *CDKN2A* are rare in multiple myeloma cell lines, which more frequently inactivate *CDKN2C*/p18, inactivation of *KDM6A* is quite common, at 30% to 40% (keatslab.org). Altogether, these data show that although *MYC* is the primary driver of Vk*MYC multiple myeloma, which is also dysregulated in approximately 40% of patients with multiple myeloma, the molecular pathogenesis of Vk*MYC multiple myeloma is heterogeneous, with some shared features with human multiple myeloma, including del(14), syntenic to human chromosome 13. More detailed genomic studies are in progress to evaluate the significance of other CNAs identified in Vk*MYC tumors, including that of monosomy 5, seen in all of the cases with monosomy 14, which has been also identified in the 5T model of multiple myeloma, with a MDR including *Fgfr3* and *Nsd2/Mmset* syntenic to human chromosome 4 (38).

Del(13) is a commonly reported abnormality in multiple myeloma; however, without a well-defined MDR its biological consequences have remained undefined. Its clinical significance has also been controversial. Del(13) was the first chromosomal abnormality to be associated with poor prognosis in multiple myeloma or with the transition from MGUS to multiple myeloma (39, 40). However, it was later found that in the absence of other confounding high risk multiple myeloma features like del(17), t(4;14), or t(14;16) translocations, del(13) by itself was not an independent prognostic factor (41). The most frequently mutated gene on chromosome 13 is *DIS3*, seen in 10% of NDMM and RMM. A recurrent mutation of codon R780K has been shown to significantly alter *DIS3* exoribonucleolytic activity, while other mutations (V504G, I845I) have little, if any effect (42). Interestingly, we found that recurrent mutations of three codons (R780, R488, and R479) are almost never associated with LOH, which, together with the absence of biallelic deletion of *DIS3*, suggests a selection for partial, but not complete inactivation of *DIS3*. Functional dissection *in vivo* of *DIS3* mutations in multiple myeloma will depend on the development of mouse models that reflect this complexity. Our work aimed therefore to dissect *in vivo,* in a biologically faithful mouse model of multiple myeloma, the contribution of available alleles to multiple myeloma pathogenesis. First, we confirmed the Knudson hypothesis and showed that *Rb1* haploinsufficiency does not promote the development of gammopathy nor contribute to multiple myeloma initiation and progression. On the other hand, biallelic *Rb1* inactivation is clearly selected by tumor cells during multiple myeloma progression in patients, in Vk*MYC mice as well as in the 5T murine model of multiple myeloma (38), and *RB1* biallelic inactivation confers very poor prognosis to patients with multiple myeloma. In contrast, loss of one copy of the *Mir15a/Mir16-1* cluster is sufficient to promote the development of monoclonal gammopathy in WT mice and drives multiple myeloma progression and extra-medullary disease dissemination in Vk*MYC mice with high penetrance, suggesting that multiple myeloma cells have acquired the ability to expand independently on a permissive BM niche. Interestingly, the presence of the *MYC* transgene is dominant over the loss of *Mir15a/Mir16-1* and clearly dictates the phenotype of the resulting tumors, which are universally multiple myeloma and not CLL. Importantly, while monosomy of chromosome 14, syntenic to human chromosome 13, spontaneously occurs in a fraction of multiple myeloma tumors from Vk*MYC mice, it never develops in Vk*MYCxMIR or Vk*MYCxMDR tumors lacking one or both copies of the *Mir15a/Mir16-1* cluster, suggesting that loss of *MIR15A/MIR16-1* expression drives the selection for chromosome 13 loss in human multiple myeloma.

Direct *Mir15a/Mir16-1* target genes have been previously identified in various model systems, and converge on regulators of cell-cycle progression. Consistently, in a comparative

analysis of murine and human multiple myeloma, we show that loss of *MIR15A/MIR16-1* is associated with increased multiple myeloma cell proliferation and more aggressive disease course. To our knowledge, this is the first time that a specific gene signature associated to *MIR15A/MIR16-1* loss is identified in murine or human tumors. The clinical significance of such increased proliferation, noted in two independent datasets and with two different methodologies, remains to be systematically determined, as well as the specific effects of *MIR15A/MIR16-1* expression on multiple myeloma survival. In previous studies, the levels of exosomal MIR-16 were found to be a significant risk factor for progression free survival, but not OS, in a univariate analysis adjusted for ISS stage and cytogenetic abnormalities, while high levels of circulating miR-16 in the serum of patients with NDMM were independent prognosticators of OS (43, 44). Furthermore, the presence of del(13) was found to be independently associated with shorter overall and progression-free survival (11) and in a new model aimed to predict risk of progression of patients with smoldering multiple myeloma, presented by the International Myeloma Working Group, t(4;14), t(14;16), 1q gain, or del(13) were identified in a multivariate Cox regression analysis to predict outcome (45).

As we defined a role for *Mir15a/Mir16-1* in the development of monoclonal gammopathy in mice, we sought to assess the contribution of del(13) in MGUS. The frequency of del(13) between MGUS and multiple myeloma was similar in most genetic subgroups, indicating that del(13) is an early event in multiple myeloma pathogenesis. Consistently, PC levels of *MIR15* and *MIR16* were not found to vary between MGUS and multiple myeloma (46). However, it was clearly underrepresented in the CCND and MAF subgroups of patients, suggesting that these MGUS patients with del(13) are more likely to rapidly progress to multiple myeloma.

Overall, we identify a role for del(13) in multiple myeloma pathogenesis in all but the MMSET subgroups, where the very low number of patients lacking del(13) reduces the power of the analysis. We also wonder whether loss of *MIR15A/MIR16-1* in the MMSET subgroup represents a prerequisite initiating event leading to the expansion of the pool of germinal center B cells amenable to acquire t(4;14) translocation. It is also possible that loss of expression of other genes on chromosome 13 drives the selection for del(13) in these tumors, which are associated with higher frequency of mutations in *DIS3* (9).

In summary, we show that one of the most common genomic abnormalities in multiple myeloma, del(13), is driven in large part by loss of one copy of the *MIR15A/MIR16-1* cluster, resulting in reduced *miR-15a/16-1* levels and increased expression of cell-cycle–regulatory genes, which drive disease progression. Therefore, while the contribution to multiple myeloma progression of other genes on chromosome 13 (e.g., *DIS3*) is likely, this study establishes a prominent role for the loss of *MIR15A/MIR16-1* in multiple myeloma pathogenesis.

## METHODS

### Mice

All *in vivo* experiments were performed under the Mayo Foundation Institutional Animal Care and Use Committee approval. The generation, characterization, and maintenance of Vk*MYC mice (GenBank accession no. MN894515), Vk*MYCxEμBCL2 mice, and of the Vk12598 transplantable line have been reported elsewhere (2, 6, 8). The B6.129S2-*Rb1*$^{tm1Tyj}$/J mice that constitutively lack one *Rb1* allele (20), here referred to as Rb$^{het}$ mice, were purchased from The Jackson Laboratory (stock 02102). Mice that constitutively carry a deletion of the *dLeu2* gene and *Mir15a/Mir16-1* cluster, here referred to as MDR mice, or the *Mir15a/Mir16-1* cluster only, MIR mice, were kindly donated by Riccardo Dalla-Favera, Institute for Cancer Genetics, Columbia University, New York, NY (15). All mice were maintained in C57BL/6J strain and crossed with each other or with Vk*MYC mice. SPEP was periodically performed on sex-matched mice as described previously (8). Mice were necropsied when moribund to assess the presence of phenotypic abnormalities by flow cytometry and IHC (6, 8). Kaplan–Meier survival curves were generated using Prism software (GraphPad Software Inc.) and compared by log-rank test.

### aCGH of Murine Multiple Myeloma Tumors

High-resolution aCGH was performed on Puregene (Qiagen) purified DNA obtained from CD138 selected (8) multiple myeloma cells from 27 mice using the SurePrint G3 Mouse CGH 244K Microarray kit (Agilent Technologies). Digestion, labeling, and hybridization steps were done according to the manufacturer's protocols with some modifications. Briefly, 1.2 μg of DNA from CD138 selected Vk*MYC multiple myeloma tumors or pooled spleens of young transgenic mice were separately digested with bovine DNase I (Ambion) for 12 minutes at room temperature. Next, random primers and exo-Klenow Fragment were used to differentially label tumor (Cy5) and reference (Cy3) genomic DNA samples (Agilent Technologies). Labeled genomic reactions were cleaned up with Microcon YM-30 Columns (Millipore) and hybridized at 65°C for 40 hours. Microarrays were scanned in a DNA Microarray Scanner (Agilent Technologies). Feature extraction was performed with Feature Extraction Software, version 9.5 (Agilent Technologies). $Log_2$ ratio data were imported and analyzed using DNA Analytics Version 4.0.85 software (Agilent Technologies). Copy-number abnormalities were calculated using aberration detection module-1 algorithm with a threshold of 7.5. A 2 probe, 0.25-$log_2$ filters were used in the aberration detection, obtaining an average genomic resolution of 17 kb. Visualization of the data aligned to mm10 was performed using IGV software (Broad Institute). The data have been submitted with GEO submission #GSE110954.

### Gene Expression Profiling of Murine Multiple Myeloma Samples

RNA from CD138-selected multiple myeloma samples was extracted from TRIzol and further purified on Purelink Micro-Mini Columns (Invitrogen), with an On-Column DNAse Digestion Step. Gene expression profiling was performed on the Affymetrix mouse 430 2.0 array following the manufacturer's suggested protocol. Datasets have been deposited to GEO under submission no. GSE111921, and further analysis was conducted on a subset of samples restricted to normal PC, Vk*MYC, Vk*MYCxMIR, or Vk*MYCxMDR tumors. Gene-level expression was derived from CEL files using custom CDF from brainarray, version 23, and RMA normalization (47). Gene-set enrichment analysis was performed using the GAGE (generally applicable gene set enrichment for pathway analysis) R package (48).

### Quantization of miR-15a Expression in Murine Multiple Myeloma Tumors

Ten nanograms of TRIzol-extracted RNA from CD138-selected multiple myeloma samples were retro-transcribed to cDNA using the TaqMan microRNA Reverse Transcription kit with RT stem-loop primers specific to mature miR-15a (assay 0389) or U6 snRNA (assay 01973, both Applied Biosystems), according to the manufacturer's instructions. The obtained cDNA was diluted 1:3 and 3 μL were amplified in a TaqMan PCR reaction using a Rotor-Gene 3000 instrument (Corbett Research). Relative miR-15a expression was normalized to U6 snRNA and quantified using the $\Delta C_t$ method (miR-15a $C_t$ – U6 $C_t$). Each sample was tested in triplicate.

### *Assessment of Chromosome 14 Ploidy by qPCR in Murine Multiple Myeloma Tumors*

The efficiencies of SYBR Green PCR reactions for each target gene were calculated on serially diluted WT DNAs, and the accepted $C_t$ range for each reaction was determined using a Rotor-Gene 3000 instrument (Corbett Research). Then, 3 ng of genomic tumor DNA were amplified in triplicate using the validated primer set. The ploidy of chr14 genes was calculated by the $2^{-\Delta\Delta C_t}$ method against Tert2, chosen as normal diploid control because it is located in a genomic locus not affected by copy number changes. Primer sequences and PCR efficiency are listed in Supplementary Table S2.

### *Copy-number–dependent Quantization of MIR15A Expression in Human Myeloma Cell Lines*

Human myeloma cell lines have been described previously (49) and were maintained in RPMI1640 supplemented with 5% FBS and glutamine without antibiotics. None of these lines are listed on the International Cell Line Authentication Committee database of commonly misidentified cell lines and are routinely fingerprinted by assessment of copy-number polymorphisms by PCR and tested for *Mycoplasma* contamination using the MycoAlert kit (Promega). The copy number for *MIR15A* in HMCL was extracted from the segmented copy number data described previously (49) using IGV, Gitools Heatmap, Export Gene Matrix TDM (50). RNA was extracted from five million logarithmically growing cells using the MirVana miRNA isolation kit (Invitrogen) following manufacturer's instructions. Relative *MIR15A* expression was normalized to the average of U6 snRNA and RNU48 snoRNA (assay 01006) expression and quantified using the $2^{-\Delta C_t}$ method. Each sample was tested in triplicate.

### *Genomic Analysis of Human Multiple Myeloma Tumors*

Clinical variables and genetic data, including whole-exome sequencing (WES), biallelic frequency segmented WES for estimation of LOH, RNA-Seq (Salmon TPM), WGS-segmented files (copy number estimates), and long-insert WGS were downloaded from MMRF CoMMpass (IA14 release data from http://research.themmrf.org). From the available samples, we focus on 924 baseline BM samples with available whole-exome or whole-genome copy number data and RNA-Seq Salmon TPM expression data. For analysis of samples at disease progression, WES on 146 samples from 121 patients from IA15 release was used.

### *Segmentation Analysis of Human Chromosome 13 in Multiple Myeloma Tumors*

Del(13) determinations are based on the total length of chromosome 13's q arm with a copy-number level, according to whole-exome segmentation file, below a given threshold, where samples with del(13) have 10% or more of the span of 13 below 1.30. This del(13) determination is positive for 98.5% of cases with loss of *MIR15A/MIR16-1*, 99% of cases with loss of *RB1*, and 100% of cases with loss of *DIS3*. To graphically search for a minimally deleted region of 13, copy-number levels from segmentation files were queried at 25k base-pair increments across all of 13, with even greater refinement for the 14q.2 band and the section of 13 surrounding *MIR15A/MIR16-1* (Fig. 5A).

## Disclosure of Potential Conflicts of Interest

S.K. Kumar is a consultant/advisory board member at Celgene, Takeda, AbbVie, Roche, GlaxoSmithKline, and Amgen. No potential conflicts of interest were disclosed by the other authors.

## Authors' Contributions

**M. Chesi:** Conceptualization, data curation, formal analysis, supervision, funding acquisition, validation, investigation, visualization, methodology, writing–original draft, writing–review, and editing. **C.K. Stein:** Conceptualization, data curation, formal analysis, writing–original draft, writing–review, and editing. **V.M. Garbitt:** Investigation. **M.E. Sharik:** Investigation. **Y.W. Asmann:** Data curation, formal analysis, investigation, and methodology. **M. Bergsagel:** Methodology. **D.L. Riggs:** Writing–review and editing. **S.J. Welsh:** Writing–review and editing. **E.W. Meermeier:** Writing–review and editing. **S.K. Kumar:** Resources, data curation, and formal analysis. **E. Braggio:** Data curation, formal analysis, investigation, methodology, writing–review, and editing. **P.L. Bergsagel:** Data curation, formal analysis, supervision, writing–review, and editing.

## Acknowledgments

We are grateful to Riccardo Dalla-Favera for providing the MIR and MDR mice. We thank W. Mike Kuehl for critical interpretation of the data. This work has been supported by the following NIH/NCI grants: CA234181 (to M. Chesi, C.K. Stein, V.M. Garbitt, M.E. Sharik, E.W. Meermeier, and M. Bergsagel), CA186781 (to M. Chesi, C.K. Stein, D.L. Riggs, and P.L. Bergsagel), CA190045 (to M. Chesi, V.M. Garbitt, and M.E. Sharik), and CA224018 (to C.K. Stein, D.L. Riggs, and P.L. Bergsagel).

The costs of publication of this article were defrayed in part by the payment of page charges. This article must therefore be hereby marked *advertisement* in accordance with 18 U.S.C. Section 1734 solely to indicate this fact.

Received December 2, 2019; revised January 14, 2020; accepted January 22, 2020; published first February 20, 2020.

## REFERENCES

1. Kuehl WM, Bergsagel PL. Molecular pathogenesis of multiple myeloma and its premalignant precursor. J Clin Invest 2012;122:3456–63.
2. Chesi M, Robbiani DF, Sebag M, Chng WJ, Affer M, Tiedemann R, et al. AID-dependent activation of a MYC transgene induces multiple myeloma in a conditional mouse model of post-germinal center malignancies. Cancer Cell 2008;13:167–80.
3. Chng WJ, Huang GF, Chung TH, Ng SB, Gonzalez-Paz N, Troska-Price T, et al. Clinical and biological implications of MYC activation: a common difference between MGUS and newly diagnosed multiple myeloma. Leukemia 2011;25:1026–35.
4. Misund K, Keane N, Stein CK, Asmann YW, Day G, Welsh S, et al. MYC dysregulation in the progression of multiple myeloma. Leukemia 2020;34:322–6.
5. Affer M, Chesi M, Chen WD, Keats JJ, Demchenko YN, Tamizhmani K, et al. Promiscuous MYC locus rearrangements hijack enhancers but mostly super-enhancers to dysregulate MYC expression in multiple myeloma. Leukemia 2014;28:1725–35.
6. Chesi M, Matthews GM, Garbitt VM, Palmer SE, Shortt J, Lefebure M, et al. Drug response in a genetically engineered mouse model of multiple myeloma is predictive of clinical efficacy. Blood 2012;120:376–85.
7. Calcinotto A, Ponzoni M, Ria R, Grioni M, Cattaneo E, Villa I, et al. Modifications of the mouse bone marrow microenvironment favor angiogenesis and correlate with disease progression from asymptomatic to symptomatic multiple myeloma. Oncoimmunology 2015;4:e1008850.
8. Chesi M, Mirza NN, Garbitt VM, Sharik ME, Dueck AC, Asmann YW, et al. IAP antagonists induce anti-tumor immunity in multiple myeloma. Nat Med 2016;22:1411–20.
9. Walker BA, Mavrommatis K, Wardell CP, Ashby TC, Bauer M, Davies FE, et al. Identification of novel mutational drivers reveals oncogene dependencies in multiple myeloma. Blood 2018;132:587–97.
10. Chiecchio L, Dagrada GP, Ibrahim AH, Dachs Cabanas E, Protheroe RK, Stockley DM, et al. Timing of acquisition of deletion 13 in plasma cell dyscrasias is dependent on genetic context. Haematologica 2009;94:1708–13.

11. Binder M, Rajkumar SV, Ketterling RP, Greipp PT, Dispenzieri A, Lacy MQ, et al. Prognostic implications of abnormalities of chromosome 13 and the presence of multiple cytogenetic high-risk abnormalities in newly diagnosed multiple myeloma. Blood Cancer J 2017;7:e600.
12. Avet-Loiseau H, Attal M, Moreau P, Charbonnel C, Garban F, Hulin C, et al. Genetic abnormalities and survival in multiple myeloma: the experience of the Intergroupe Francophone du Myelome. Blood 2007;109:3489–95.
13. Rawstron AC, Bennett FL, O'Connor SJ, Kwok M, Fenton JA, Plummer M, et al. Monoclonal B-cell lymphocytosis and chronic lymphocytic leukemia. N Engl J Med 2008;359:575–83.
14. Fonseca R, Oken MM, Harrington D, Bailey RJ, Van Wier SA, Henderson KJ, et al. Deletions of chromosome 13 in multiple myeloma identified by interphase FISH usually denote large deletions of the q arm or monosomy. Leukemia 2001;15:981–6.
15. Klein U, Lia M, Crespo M, Siegel R, Shen Q, Mo T, et al. The DLEU2/miR-15a/16–1 cluster controls B cell proliferation and its deletion leads to chronic lymphocytic leukemia. Cancer Cell 2010;17:28–40.
16. Lindner SE, Lohmuller M, Kotkamp B, Schuler F, Knust Z, Villunger A, et al. The miR-15 family reinforces the transition from proliferation to differentiation in pre-B cells. EMBO Rep 2017;18:1604–17.
17. Roccaro AM, Sacco A, Thompson B, Leleu X, Azab AK, Azab F, et al. MicroRNAs 15a and 16 regulate tumor proliferation in multiple myeloma. Blood 2009;113:6669–80.
18. Bergsagel PL, Kuehl WM. Degree of focal immunoglobulin heavy chain locus deletion as a measure of B-cell tumor purity. Leukemia 2013;27:2067–8.
19. Chavan S, He J, Tytarenko R, Deshpande S, Patel P, Bailey M, et al. Bi-allelic inactivation is more prevalent at relapse in multiple myeloma, identifying RB1 as an independent prognostic marker. Blood Cancer J 2017;7:e535.
20. Jacks T, Fazeli A, Schmitt EM, Bronson RT, Goodell MA, Weinberg RA. Effects of an Rb mutation in the mouse. Nature 1992;359:295–300.
21. Radl J, Hollander CF. Homogeneous immunoglobulins in sera of mice during aging. J Immunol 1974;112:2271–3.
22. Roccaro AM, Sacco A, Maiso P, Azab AK, Tai YT, Reagan M, et al. BM mesenchymal stromal cell-derived exosomes facilitate multiple myeloma progression. J Clin Invest 2013;123:1542–55.
23. Jia X, Li X, Shen Y, Miao J, Liu H, Li G, et al. MiR-16 regulates mouse peritoneal macrophage polarization and affects T-cell activation. J Cell Mol Med 2016;20:1898–907.
24. Khalife J, Ghose J, Martella M, Viola D, Rocci A, Troadec E, et al. MiR-16 regulates crosstalk in NF-kB tolerogenic inflammatory signaling between myeloma cells and bone marrow macrophages. JCI Insight 2019;4(21):e129615.
25. Calin GA, Cimmino A, Fabbri M, Ferracin M, Wojcik SE, Shimizu M, et al. MiR-15a and miR-16–1 cluster functions in human leukemia. Proc Natl Acad Sci U S A 2008;105:5166–71.
26. Bhan S, Chuang A, Negi SS, Glazer CA, Califano JA. MAGEA4 induces growth in normal oral keratinocytes by inhibiting growth arrest and apoptosis. Oncol Rep 2012;28:1498–502.
27. Sun Q, Chen X, Zhou Q, Burstein E, Yang S, Jia D. Inhibiting cancer cell hallmark features through nuclear export inhibition. Signal Transduct Target Ther 2016;1:16010.
28. Schmidt J, Braggio E, Kortuem KM, Egan JB, Zhu YX, Xin CS, et al. Genome-wide studies in multiple myeloma identify XPO1/CRM1 as a critical target validated using the selective nuclear export inhibitor KPT-276. Leukemia 2013;27:2357–65.
29. Rodriguez-Bravo V, Pippa R, Song WM, Carceles-Cordon M, Dominguez-Andres A, Fujiwara N, et al. Nuclear pores promote lethal prostate cancer by increasing POM121-driven E2F1, MYC, and AR nuclear import. Cell 2018;174:1200–15.
30. Neuenkirchen N, Chari A, Fischer U. Deciphering the assembly pathway of Sm-class U snRNPs. FEBS Lett 2008;582:1997–2003.
31. Lee AS, Kranzusch PJ, Cate JH. eIF3 targets cell-proliferation messenger RNAs for translational activation or repression. Nature 2015;522:111–4.
32. Cimmino A, Calin GA, Fabbri M, Iorio MV, Ferracin M, Shimizu M, et al. miR-15 and miR-16 induce apoptosis by targeting BCL2. Proc Natl Acad Sci U S A 2005;102:13944–9.
33. Sun CY, She XM, Qin Y, Chu ZB, Chen L, Ai LS, et al. miR-15a and miR-16 affect the angiogenesis of multiple myeloma by targeting VEGF. Carcinogenesis 2013;34:426–35.
34. Zhang L, Zhou L, Shi M, Kuang Y, Fang L. Downregulation of miRNA-15a and miRNA-16 promote tumor proliferation in multiple myeloma by increasing CABIN1 expression. Oncol Lett 2018;15:1287–96.
35. Lakshman A, Paul S, Rajkumar SV, Ketterling RP, Greipp PT, Dispenzieri A, et al. Prognostic significance of interphase FISH in monoclonal gammopathy of undetermined significance. Leukemia 2018;32:1811–5.
36. Bergsagel PL, Kuehl WM, Zhan F, Sawyer J, Barlogie B, Shaughnessy J Jr. Cyclin D dysregulation: an early and unifying pathogenic event in multiple myeloma. Blood 2005;106:296–303.
37. Hose D, Reme T, Hielscher T, Moreaux J, Messner T, Seckinger A, et al. Proliferation is a central independent prognostic factor and target for personalized and risk-adapted treatment in multiple myeloma. Haematologica 2011;96:87–95.
38. Maes K, Boeckx B, Vlummens P, De Veirman K, Menu E, Vanderkerken K, et al. The genetic landscape of 5T models for multiple myeloma. Sci Rep 2018;8:15030.
39. Avet-Loiseau H, Li JY, Morineau N, Facon T, Brigaudeau C, Harousseau JL, et al. Monosomy 13 is associated with the transition of monoclonal gammopathy of undetermined significance to multiple myeloma. Intergroupe Francophone du Myelome. Blood 1999;94:2583–9.
40. Tricot G, Barlogie B, Jagannath S, Bracy D, Mattox S, Vesole DH, et al. Poor prognosis in multiple myeloma is associated only with partial or complete deletions of chromosome 13 or abnormalities involving 11q and not with other karyotype abnormalities. Blood 1995;86:4250–6.
41. Gutierrez NC, Castellanos MV, Martin ML, Mateos MV, Hernandez JM, Fernandez M, et al. Prognostic and biological implications of genetic abnormalities in multiple myeloma undergoing autologous stem cell transplantation: t(4;14) is the most relevant adverse prognostic factor, whereas RB deletion as a unique abnormality is not associated with adverse prognosis. Leukemia 2007;21:143–50.
42. Tomecki R, Drazkowska K, Kucinski I, Stodus K, Szczesny RJ, Gruchota J, et al. Multiple myeloma-associated hDIS3 mutations cause perturbations in cellular RNA metabolism and suggest hDIS3 PIN domain as a potential drug target. Nucleic Acids Res 2014;42:1270–90.
43. Manier S, Liu CJ, Avet-Loiseau H, Park J, Shi J, Campigotto F, et al. Prognostic role of circulating exosomal miRNAs in multiple myeloma. Blood 2017;129:2429–36.
44. Rocci A, Hofmeister CC, Geyer S, Stiff A, Gambella M, Cascione L, et al. Circulating miRNA markers show promise as new prognosticators for multiple myeloma. Leukemia 2014;28:1922–6.
45. Miguel JS, Mateos MV, Gonzalez V, Dimopoulos MA, Kastritis E, Hajek R, et al. Updated risk stratification model for smoldering multiple myeloma (SMM) incorporating the revised IMWG diagnostic criteria. J Clin Oncol 2019;37(15_suppl):8000.
46. Seckinger A, Meissner T, Moreaux J, Benes V, Hillengass J, Castoldi M, et al. miRNAs in multiple myeloma–a survival relevant complex regulator of gene expression. Oncotarget 2015;6:39165–83.
47. Dai M, Wang P, Boyd AD, Kostov G, Athey B, Jones EG, et al. Evolving gene/transcript definitions significantly alter the interpretation of GeneChip data. Nucleic Acids Res 2005;33:e175.
48. Luo W, Friedman MS, Shedden K, Hankenson KD, Woolf PJ. GAGE: generally applicable gene set enrichment for pathway analysis. BMC Bioinformatics 2009;10:161.
49. Keats JJ, Fonseca R, Chesi M, Schop R, Baker A, Chng WJ, et al. Promiscuous mutations activate the noncanonical NF-kappaB pathway in multiple myeloma. Cancer Cell 2007;12:131–44.
50. Robinson JT, Thorvaldsdottir H, Winckler W, Guttman M, Lander ES, Getz G, et al. Integrative genomics viewer. Nat Biotechnol 2011;29:24–6.